

In-situ study of growth of carbon nanotube forests on conductive CoSi₂ support

B. C. Bayer, C. Zhang, R. Blume, F. Yan, M. Fouquet, C. T. Wirth, R. S. Weatherup, L. Lin, C. Baetz, R. A. Oliver, A. Knop-Gericke, R. Schlögl, S. Hofmann, and J. Robertson

Citation: [Journal of Applied Physics](#) **109**, 114314 (2011); doi: 10.1063/1.3592234

View online: <http://dx.doi.org/10.1063/1.3592234>

View Table of Contents: <http://scitation.aip.org/content/aip/journal/jap/109/11?ver=pdfcov>

Published by the [AIP Publishing](#)

Articles you may be interested in

[Effect of hydrogen pretreatment on the spin-capability of a multiwalled carbon nanotube forest](#)

J. Vac. Sci. Technol. B **31**, 06F102 (2013); 10.1116/1.4825116

[Low temperature growth of ultra-high mass density carbon nanotube forests on conductive supports](#)

Appl. Phys. Lett. **103**, 073116 (2013); 10.1063/1.4818619

[Use of plasma treatment to grow carbon nanotube forests on TiN substrate](#)

J. Appl. Phys. **109**, 114312 (2011); 10.1063/1.3587234

[Manipulation of the catalyst-support interactions for inducing nanotube forest growth](#)

J. Appl. Phys. **109**, 044303 (2011); 10.1063/1.3549813

[Effect of catalyst oxidation on the growth of carbon nanotubes by thermal chemical vapor deposition](#)

J. Appl. Phys. **100**, 104321 (2006); 10.1063/1.2364381



AIP | Journal of Applied Physics

Meet The New Deputy Editors

	Christian Brosseau		Laurie McNeil		Simon Phillpot
---	---------------------------	---	----------------------	---	-----------------------

In-situ study of growth of carbon nanotube forests on conductive CoSi₂ support

B. C. Bayer,¹ C. Zhang,¹ R. Blume,^{2,a)} F. Yan,¹ M. Fouquet,¹ C. T. Wirth,¹ R. S. Weatherup,¹ L. Lin,¹ C. Baehtz,³ R. A. Oliver,⁴ A. Knop-Gericke,² R. Schlögl,² S. Hofmann,¹ and J. Robertson^{1,b)}

¹Department of Engineering, University of Cambridge, Cambridge, CB3 0FA, United Kingdom

²Fritz-Haber-Institut der Max-Planck-Gesellschaft, D-14195 Berlin-Dahlem, Germany

³Institute of Ion Beam Physics and Materials Research, Helmholtz-Zentrum Dresden-Rossendorf, D-01314 Dresden, Germany

⁴Department of Materials Science and Metallurgy, University of Cambridge, Cambridge, CB2 3QZ, United Kingdom

(Received 26 January 2011; accepted 13 April 2011; published online 9 June 2011)

The growth of high density vertically aligned carbon nanotube forests on conductive CoSi₂ substrate layers is characterized by *in situ* x-ray photoemission spectroscopy and x-ray diffraction. We use *in situ* silicidation to transform as loaded, low conductivity CoSi supports to highly conductive CoSi₂ during nanotube growth. These cobalt silicide films are found to be stable against oxidation and carbide formation during growth and act as an excellent metallic support for growth of aligned nanotubes, resembling the growth on the insulating Fe/Al₂O₃ benchmark system. The good catalytic activity is attributed to interfacial reactions of the Fe catalyst particles with the underlying CoSi₂ support. We obtain ohmic conduction from the support layer to the carbon nanotube forest. © 2011 American Institute of Physics. [doi:10.1063/1.3592234]

I. INTRODUCTION

Carbon nanotubes (CNTs) are a promising material for use as interconnects between transistors in integrated circuits.^{1–3} This is due to their very high current carrying capacity of $\sim 10^9$ A/cm², resistance to electromigration, and their ability to be grown in deep, high aspect ratio holes. These properties are a direct advantage over the presently used Cu when feature sizes are further scaled down in vertical interconnects (vias), which connect the various metallization levels in integrated circuits. This application requires the CNTs to be grown by chemical vapor deposition (CVD) in very high density vertically-aligned forests.^{4–11} There has been great progress in growing such forests on insulating substrates such as Al₂O₃ or SiO₂ (Refs. 12–21). However, the growth of such forests of CNTs on conductive substrates is a more challenging process due to the much higher surface energy of metals than insulating oxides (Table I). The higher surface energy inhibits the catalyst film from transforming itself into a series of nanoparticles.^{22–26} In addition, the metallic support must retain its conductivity/functionality during the CVD processes at elevated temperatures in the presence of reactive gases, but metals are often reactive themselves under such conditions.²⁷ This means that supports must possess both favorable surface energetics for high density nanoparticle formation and a chemical stability against carbide-formation (from carbon source gas) or oxidation (from residual oxygen or water).

Ta has been used by some groups as a metallic support, because it is a useful diffusion barrier material already used in microelectronics. Good CNT growth was achieved on this metal. However, detailed *in situ* study of CNT growth on Ta found that Ta could be easily oxidized by residual oxygen in the presence of some growth catalysts like Fe, and that Ta also tended to form Ta carbide.²⁷ This suggests the use of metallic compounds. TiN and TaN are widely used in microelectronics and CNTs have been found to grow on these supports.^{25,28} However, the nitride surfaces are easily oxidized.^{28,29} This suggests silicides as an alternative due to their high stability. CoSi₂ is a commonly used contact material in integrated circuit fabrication.^{30–37} We recently found that CoSi₂ is a promising candidate to combine favorable surface energetics and chemical stability.²⁶

In this paper, we evaluate Co-silicides further as supports for high density CNT growth by employing *in situ* chemical and structural characterization techniques to study the evolution of the silicide-catalyst-gas system during CNT

TABLE I. Surface energies of solid metals, metallic compounds and oxides, in J/m², from Ref. 26.

	Experiment	Theory
Ni	2.08	2.01
Co	2.22	2.77
Fe	2.12, 1.72	2.22
TiN		1.6, 1.40
CoSi ₂	0.72–0.8	1.65
NiSi ₂		1.13
SiO ₂	0.043–0.11	
Al ₂ O ₃	0.06–0.1	0–0.1
MgO	0.1	

^{a)}Present address: Division Solar Energy Research, Helmholtz-Zentrum Berlin for Materials and Energy, D-12487 Berlin, Germany.

^{b)}Author to whom correspondence should be addressed. Electronic: jr214@hermes.cam.ac.uk.

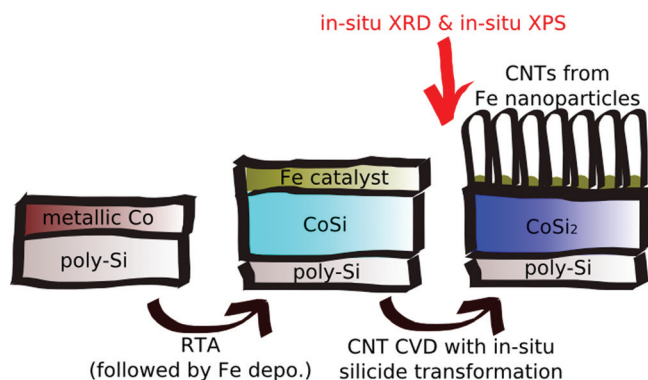


FIG. 1. (Color online) Schematic of *in situ* silicidation from low conductivity CoSi to highly conductive CoSi₂ during CNT growth.

forest growth. We correlate our findings with the electrical characterization of silicide-supported CNT forests. To keep the thermal budget of the silicide films sufficiently low (to avoid e.g., film inversion or mixing^{30–32}), we initially deposit the Fe catalyst onto not fully crystallized, low conductivity Co-monosilicide (CoSi) and then transform it to the high conductivity phase Co-disilicide (CoSi₂) *in situ* during the CNT growth (Fig. 1). Thereby, we show that we promote growth of the CNTs onto a fresh, *in situ* formed film microstructure and surface, hence limiting the effects of transporting the films in air during process steps.

II. EXPERIMENTAL DETAILS

The silicide films were prepared by the low pressure CVD of ~ 200 nm poly-Si onto polished single crystalline Si (100) wafers, followed by sputter deposition of a ~ 15 nm Co layer. This structure was capped by a TiN layer and annealed by rapid thermal annealing (RTA) at temperatures under 500 °C for under three min, followed by the removal of the TiN capping layer. The annealing led to interdiffusion of the Co and the Si and the formation of CoSi (see below). The TiN capping layer promotes the development of a smoother silicide surface. Usually a second, further annealing step is then employed to transform the CoSi into high conductivity CoSi₂ (Refs. 30–32). We can avoid this second step as we transform CoSi into CoSi₂ simultaneously with the CNT growth.

After transport of CoSi wafers in air, a ~ 1 nm Fe catalyst layer was deposited onto the samples by thermal evaporation. CNT growth and simultaneous silicide transformation was conducted in atmospheric, near-atmospheric or low pressure CVD conditions as summarized in Table II. The

structural evolution of samples was monitored during near-atmospheric CVD by *in situ* x-ray diffractometry (XRD) and x-ray reflectivity (XRR).²⁷ *In situ* (grazing incidence) XRD and XRR was measured at ROBL/BM20, operated by the Helmholtz-Zentrum Dresden Rossendorf, at the European Synchrotron Radiation Facility (XRD scans plotted at 1.541 Å). The evolution of the surface chemistry of samples was monitored during low pressure CVD by *in situ* x-ray photoelectron spectroscopy (XPS).^{38,39} *In situ* XPS was measured at the ISSS end station of the FHI-MPG at BESSY II. For details of the *in situ* XPS apparatus, see Ref. 40.

Post-growth analysis of samples was carried out by Scanning Electron Microscopy (SEM, FEI Philips XL30 sFEG) and Raman spectroscopy (Renishaw 1000, 514 nm excitation). Electrical measurements were carried out with a two terminal probe station (Cascade with Agilent Technologies B1500A semiconductor parameter analyzer) as well as with a conductive tip IV-AFM setup (Veeco Dimension 3100 with Nanoscope V controller and Veeco Extended TUNA module with a Pt-Ir coated tip).

III. RESULTS

A. Growth

Multi-walled nanotube forests of tens of μm height are found to grow easily on the Co-silicide support under the atmospheric and low-pressure conditions listed in Table II. This is confirmed by SEM (Fig. 2) and Raman spectroscopy (not shown), consistent with our previous report.²⁶ The nanotube density is estimated at $\sim 10^{10}$ CNTs/cm² from the SEM micrographs.⁴¹ Near-atmospheric CVD conditions lead to somewhat lower density CNT growth with less alignment (not shown), but are interesting because they allow *in situ* XRD.

B. XRD

Figure 3(a) shows that the structural evolution of the silicide during near-atmospheric pressure CVD, as measured by *in situ* XRD (information depth ~ 70 nm, due to grazing incidence setup), is as expected from the process flow in Fig. 1: The as-loaded silicide film shows reflections corresponding to poly-Si⁴² and a small contribution of two reflections which can be assigned to CoSi (Ref. 42). The small magnitude of the CoSi signal is ascribed to low crystallinity of the monosilicide film after its formation by the low temperature RTA. The Fe is not visible in XRD due to its very small film thickness and a partial reflection overlap.

TABLE II. Summary of CVD conditions. Low pressure and near-atmospheric pressure CVD were conducted in custom-built reaction chambers with heating stages (cold wall). Atmospheric pressure CVD was done in a custom-built quartz tube furnace (hot wall).

	Ramp	Pre-treatment	Growth	In-situ characterization
Low pressure	in 0.1–0.5 mbar NH ₃ at ~ 300 °C/min	in 0.1–0.5 mbar NH ₃ at ~ 650 °C for 10–60 min	add 10% C ₂ H ₂ to pre-treatment conditions for 20–30 min	In-situ XPS at BESSY II
Near-atmospheric pressure	in 150–250 mbar Ar:H ₂ at ~ 100 °C/min	in 150–250 mbar Ar:H ₂ at ~ 650 °C for 90 min	add $\sim 2\%$ C ₂ H ₂ to pre-treatment conditions for 90 min	In-situ XRD and XRR at ROBL/ESRF
Atmospheric pressure	in 1000 mbar Ar at 20 °C/min	in 1000 mbar Ar:H ₂ at 650 °C–750 °C for three min	add 2% C ₂ H ₂ to pre-treatment conditions for 30 min	-

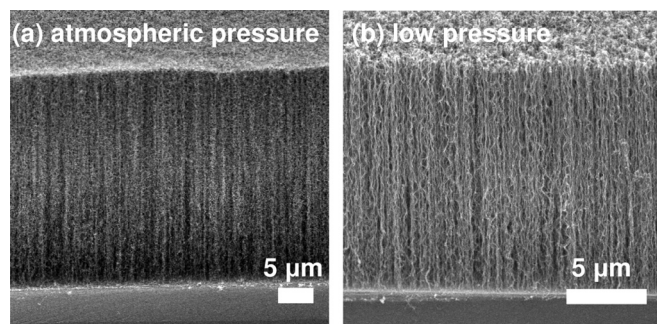


FIG. 2. Typical CNT forest growth results with the CVD conditions from Table II (SEM micrographs at a tilt of $\sim 60^\circ$). In particular, (a) shows atmospheric pressure CVD at 650°C . (b) shows low pressure CVD at ~ 0.1 mbar with 30 min pretreatment and 30 min growth at $\sim 650^\circ\text{C}$ (Ref. 41).

During pretreatment in H_2/Ar at $\sim 650^\circ\text{C}$ we find that most poly-Si related reflections develop a shoulder to higher angles. We ascribe this to the formation of CoSi_2 . The reflections of the formed CoSi_2 (Ref. 42) become fully visible in the post-deposition scan with its higher signal/noise ratio. As

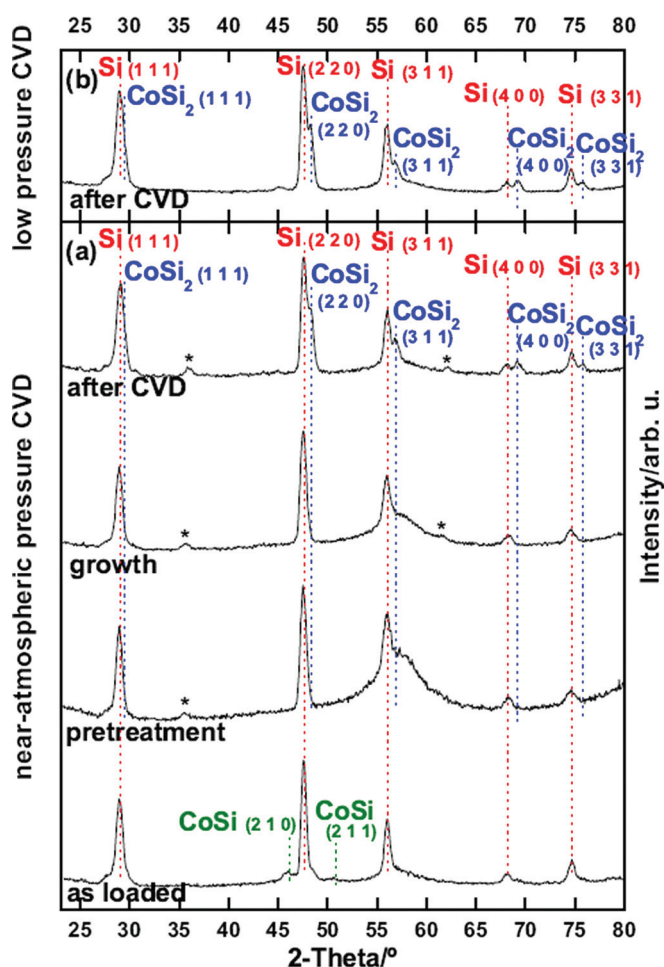


FIG. 3. (Color online) (a) Process-step resolved structural evolution of silicide supports during near-atmospheric pressure CVD as measured by *in situ* XRD. CoSi in the as loaded samples is transformed into CoSi_2 during the CNT CVD. * designates reflections which may be related to a minor Co-oxide/silicate contribution. (b) Ex-situ XRD scan of a sample after low pressure CVD. (Diffraction patterns are plotted for 1.541 \AA x-ray wavelength.)

the CoSi_2 appears during CVD the CoSi reflections disappear, following the established silicidation model for Co-silicides of $(\text{poly-Si}/\text{Co} \rightarrow \text{Co}_2\text{Si} \rightarrow \text{CoSi} \rightarrow \text{CoSi}_2)$ (Refs. 30–32). From additional XRR measurements (not shown) we estimate a silicide thickness of ~ 20 nm. In some samples, we find two additional low intensity reflections which remain ambiguous to assign. They may be related to Co-silicate or Co-oxide.⁴² This is ascribed to the silicide or residual Co on the surface reacting with residual oxygen or water in the chamber. We note however that this contribution is small and limited to some near-atmospheric samples. For low pressure CVD, post-growth XRD scans show similarly the formation of CoSi_2 , but without any possible Co-oxide/-silicate contributions [Fig. 3(b)]. This is due to the cleaner environment in low pressure CVD (base pressure $\sim 10^{-6}$ mbar) compared to a greater oxygen or water contamination in the near-atmospheric pressure system.

Our XRD data confirms that we indeed form crystalline CoSi_2 *in situ* during the CVD process, consistent with our process flow. Notably, in none of our samples we find uncalled-for formation of carbides, other material interactions such as catalyst-support-alloying or complete transformation of the “bulk” of the film into an oxide, as occurred for the case of CNT growth on Ta under similar conditions.²⁷

C. XPS

We use surface sensitive (1–3 nm maximum information depth) *in situ* XPS to measure the chemical state of the support, the Fe catalyst and the growing nanotubes during low pressure CVD, to complement the XRD measurements of the structural evolution of the “bulk” silicides. Figure 4 shows that the surface of the as-loaded monosilicide consists of oxidized Co (779.9 eV and 781.6 eV) and Si-oxide (102.6 eV).^{43–45} This is expected, as the samples were transported in air between process steps and measurements and Co-silicide is known to form a thin native oxide when exposed to ambient conditions.³⁰ The Co-oxide might also stem from unreacted Co residues from the low temperature RTA silicidation. The Fe catalyst film is also completely oxidized, exhibiting a satellite structure in the XPS spectra which suggests that additionally OH groups are present (Fe^{2+} : 709.2 eV, Fe^{3+} : 710.6 eV).^{46,47}

During pretreatment (heating in NH_3) the surface Co is almost completely reduced (778.2 eV), while the Si stays oxidized.⁴⁸ The latter is also expected as it is known that metallic Co cannot reduce SiO_2 during silicidation (unlike e.g., Ti³⁰), nor is SiO_2 affected by NH_3 .³⁹ We find however, as in XRD, that CoSi_2 is formed on the surface during the pretreatment (development of peaks at 778.9 eV in Co2p and ~ 99.7 eV in Si2p,⁴⁹) again in accordance with our process flow. This means that when we introduce C_2H_2 into the CVD chamber in the next step, CNTs are at least partially growing on a freshly formed CoSi_2 surface, possibly where the native oxide is thinnest. We measure corresponding electrical characteristics below.

During annealing, the Fe catalyst layer does split into nanoparticles²⁶ but we find that it is only partially reduced (reduction evidenced by the appearance of a component at

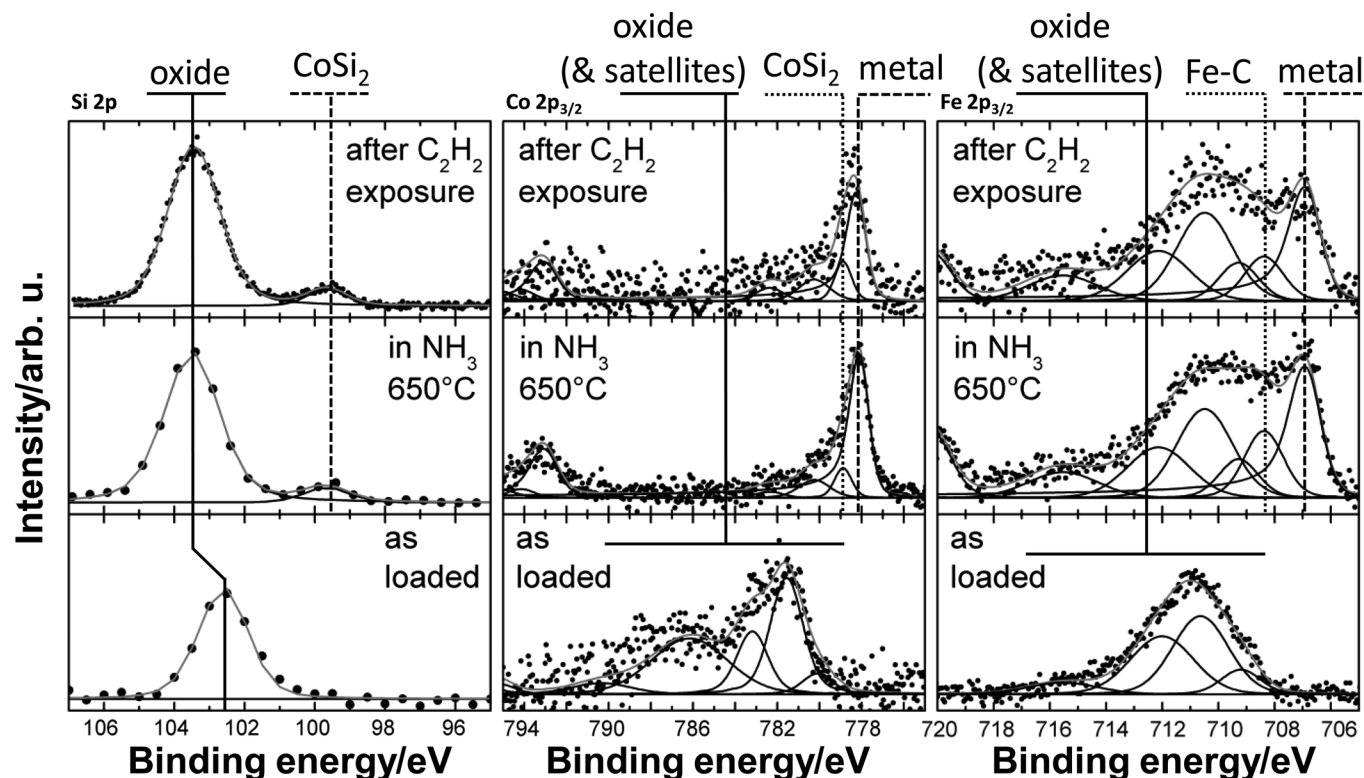


FIG. 4. (from left to right) *In situ* XPS spectra of the Si 2p, Co 2p_{3/2} and Fe 2p_{3/2} regions showing the evolution of the surface (Fe, Co; E_{kin}(e⁻) = 150 eV) and near surface (Si; E_{kin}(e⁻) = 1000 eV) chemistry under low pressure CVD.

706.9 eV). This is in contrast to Fe during NH₃ pretreatment on SiO₂ where the Fe is fully reduced.³⁸ The silicide support seems to retain some of the Fe in its oxidized form. The formation of an interfacial Fe oxide layer was also found for Fe-catalyzed CNT growth on Al₂O₃, which is the most successful support/catalyst combination for high density CNT growth on an insulator so far.³⁸ On Al₂O₃ the interfacial oxide layer pins down the Fe, preventing the catalyst nanoparticles from excessive sintering and in turn allowing high density CNT growth to occur. We have shown previously by *ex-situ* AFM study that CoSi₂ similarly seems to inhibit the sintering of Fe nanoparticles, which in turn allows the efficient growth of CNT forests.²⁶ Now, our XPS data suggests that the Fe nanoparticles become stabilized on the CoSi₂ surface by an interfacial reaction, in a similar fashion as occurs for Fe on Al₂O₃.^{38,50,51}

When we add 10% C₂H₂ to the NH₃, the XPS C1s spectra (not shown) evidence a rapid evolution of sp²- and sp³-carbon related peaks, typical of CNT growth.^{38,39} In fact, the growth rate of the obtained forests from standard low pressure CVD [Fig. 2(b)] is too fast to allow the acquisition of high resolution XPS scans of the silicide during C₂H₂ exposure. After growth, the 10–40 μm high CNT layers prevent the escape of photoelectrons from the silicide/CNT interface to the XPS detector, so no information about the post-CVD silicide surface can be gained through the forests. Therefore, to measure the chemical state of the interface during growth, we deliberately only pulse the C₂H₂, leading to a sparse growth of CNTs, but allowing us to probe the silicide surface. After C₂H₂ exposure, we find on the surface a

mixture of metallic Co and CoSi₂ plus unreduced SiO₂, but no Co- or Si-carbides. The state of the Fe did not significantly change with C₂H₂ exposure. As noted above, we cross-checked the XPS data with post-growth XRD of the same samples [Fig. 3(b)], where we find only poly-Si and CoSi₂ in the films. This implies that the oxides seen in XPS are only thin surface oxides, which do not extend into the bulk of the film. This is also corroborated by the electrical characterization, below.

XPS shows that the silicide surface consists of metallic Co and Co-silicide after the reducing pretreatment stage. The metallic Co could be due to either unreacted Co residues or to Co originating from the break-up of the silicide due to the formation of the thin native oxide layer. Morphologically, the surface is composed of nano-sized domains.²⁶ Metallic cobalt and cobalt silicide in nanoparticle form are both active CNT catalysts.⁵² Thus, it is not surprising that testing bare silicide samples without Fe catalyst leads to CNT growth under CVD conditions. The CNT yield is however significantly lower and only sparse, spaghetti-like CNTs grow (not shown). Nevertheless, this might suggest also a beneficial interplay between the Fe catalyst and the Co,^{53–55} responsible for the excellent support properties of Co-silicides for CNT growth.

D. Electrical data

We now correlate the structural and chemical evolution of the Co-silicide samples with two-terminal I-V measurements. Figure 5(a) shows I-V curves corresponding to bare silicide samples (no Fe catalyst) as loaded, after pretreatment

and after exposure to atmospheric CVD conditions at 650°C. As there was no Fe catalyst present, no CNT forest was grown and the small amount of CNTs grown from residual Co was stripped from the samples by adhesive tape. All films show a linear I-V relationship, implying that we form ohmic contacts with the probe tips. Hence, any oxide from transport in air is restricted to a ~ 1 nm thick layer, corroborating the characterization results above. We find that the annealing and CVD step roughly halve the resistance in the silicide film. This is consistent with a transition from as-loaded, low conductivity CoSi films to a high conductivity CoSi₂ phase in the annealed and CVD processed films, confirming our XRD assignments.^{30–32} It also confirms our XRD result that no other high resistivity phases such as oxides or carbides are formed in the support during CVD.

We extended the I-V characterization to include the CNTs by placing a copper TEM grid as a top electrode onto the forest surface, spreading the applied load from the probe tips over a large area to avoid squeezing/scratching off of CNTs. Gently contacting the grid with one probe tip leaves the forests intact, as checked by inspection of the forests after removal of the grid. The other probe tip was in direct contact to the Co-silicide film. Figure 5(b) shows that the resistance when contacting through the forest *and* the silicide compared to direct contact to the silicide increased only by a factor of two and developed only a slight nonlinearity. Considering the uncertainty in actual contact area on the forest, this shows that the CNTs do not significantly increase the overall system resistance.

The extraction of quantitative values from this data is complex, as several resistors in series contribute to it, most importantly the substrate-tube contact resistance, the internal tube resistance and the tube-(grid-)probe tip contact resistance (plus the resistances of the silicide film, the silicide-probe contact and the measurement setup). Furthermore, the macroscopic dimensions of probe station tips ($\sim \mu\text{m}$ radius) compared to the nanoscopic CNT diameters inhibit extraction of tube-specific values. Therefore, we refine our measurements by employing an IV-AFM setup using a conductive AFM tip (~ 20 nm radius) as the top contact to the forest. The AFM feedback allows contacting of the CNTs with the application of a greatly reduced force compared to the macroscopic probe station tips, hence completely avoiding any squeezing, scratching off or damaging of the forest. We find linear, ohmic IV characteristics [Fig. 5(c)] with measured resistances of (80 ± 60) k Ω . With a tube density of $\sim 10^{10}$ CNTs/cm² and the ~ 20 nm radius AFM tip, we estimate one to ten tubes to be in contact with the AFM tip. This translates to a resistance per tube (including internal tube resistance and contact resistances to support and probe tip) on the order of a few tens to a few hundreds of k Ω . Such values compare well to recent studies on CNT forest growth on conductive supports^{11,27} and confirm our probe station result that the CNTs are highly conductive.

Both low pressure and atmospheric pressure CVD give similar electrical results, indicating that despite the much higher residual gas contamination level in atmospheric pressure (especially residual oxygen and adsorbed water) cobalt

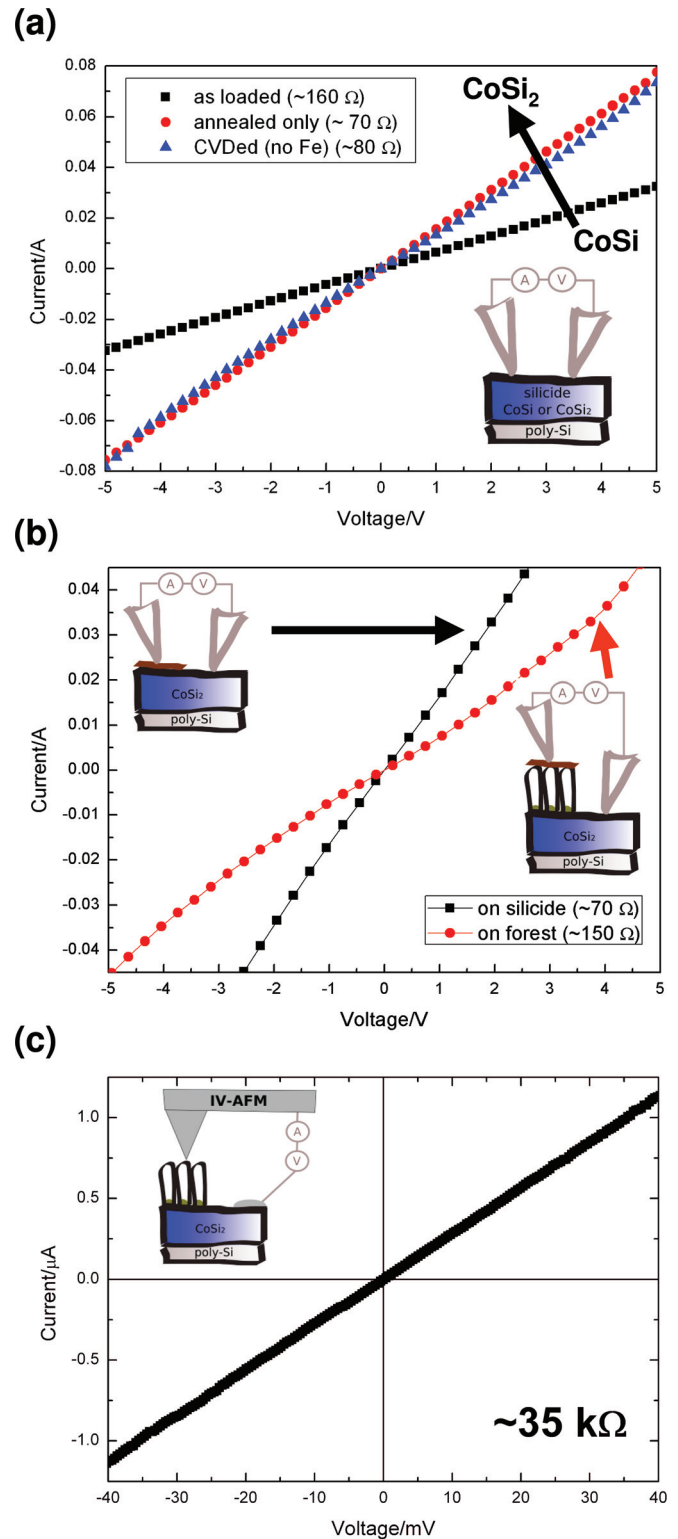


FIG. 5. (Color online) I-V characteristics of atmospheric pressure CVD samples: (a) Macroscopic probe station measurements of CVD processed samples from as loaded (black) and only pretreated (red) to fully CVDed (blue) state. Note that as no Fe was on the samples the measurements do not include a contribution from CNTs. (b) Post-CVD probe station measurements comparing conduction through the silicide only (black) to conduction through the silicide *and* the CNT forest (red). (c) Post-CVD IV-AFM measurements through silicide *and* CNT forest [with only microscopic top contact area compared to (b)].

silicide is a chemically very stable support compared to other potential support materials in microelectronics [e.g. compared to Ta (Ref. 27)].

IV. DISCUSSION

We finally remark that any processing which involves exposure of the support-catalyst interface to ambient air conditions is detrimental to obtaining very low contact resistance. This is due to Co-silicides being susceptible to native oxidation similar to pristine Si. Also, a too high residual oxygen or water partial pressure during annealing (or in our case CVD) can hinder full silicidation.^{30–32} Therefore, low pressure processes are preferable compared to atmospheric pressure furnace processes. Nevertheless, we found no significant differences in electrical properties from our low and atmospheric pressure CVD and hence conclude that the limiting contact influences in our samples come from other sources. In our low pressure CVD we saw that CNT growth proceeded partially on a freshly formed CoSi₂ surface (from XPS), but most of the already existing thin SiO₂ layer from sample transport in air was not removed in the CVD conditions. We attribute the main contact resistance to this layer, which was formed during sample exposure to air.

Hence, the following measures could further decrease the formation of any oxide barriers which limit the silicide-CNT contact performance: (1). Cluster processing of support deposition/anneal, catalyst film deposition and CNT CVD without exposing samples to ambient at any stage. This would however be a cost intensive solution. (2). Use of catalyst layer as capping layer: If the support is deposited and annealed and the catalyst is deposited subsequently without breaking vacuum, a thick enough catalyst layer could prevent oxidation of the support surface when samples are then exposed to air. The catalyst is reduced by the pretreatment gases during CVD and growth of CNTs on a pristine support surface may then be possible. However, this would require a rather thick, continuous catalyst layer, which is detrimental to the small catalyst particle sizes in high density, small diameter CNT growth. Specifically, for our process flow and our obtained data, removing the remaining residual surface Co and the surface SiO₂ by wet etches (where both etches need to be selective with respect to the silicide) before deposition of a sufficiently thick catalyst film could decrease any contact resistance from the thin SiO₂. We are currently working toward optimization of such etching processes.

Our data suggests that purely in terms of a catalyst support, CoSi₂ is a preferable support, being of low resistivity and of low reactivity to bulk oxidation or carbide formation. NiPtSi is the preferred silicide in modern VLSI because it uses less Si than a disilicide³⁶ and hence, NiPtSi is a further future CNT support candidate. TiN is the preferred contact metal below the ‘metal-one’ level in VLSI, because of its work function. We have previously analyzed CNT growth on TiN.²⁹ However, TiN has the disadvantage that it is more easily oxidized while oxidative plasmas and similar treatments are valuable for increasing the CNT forest density and enforcing the relevant root growth.^{56,57} Further work will be needed to deal with the application of such treatments also to CoSi₂ supports in order to improve the CNT forest density.

V. CONCLUSION

We have characterized Fe catalyzed CNT growth on conductive CoSi₂ support in terms of structure and chemistry of

the support and catalyst system. We employ *in situ* silicidation to transform low conductivity CoSi to highly conductive CoSi₂ during CNT forest CVD. We have confirmed that CoSi₂ films are stable against (bulk) oxidation and carbide formation during CVD, and they provide an excellent conductive support material for vertically aligned CNT growth, resembling growth on the insulating Fe/Al₂O₃ benchmark system. Our data implies that the excellent catalytic capabilities arise from an interfacial reaction of the Fe catalyst particles with the underlying Co/Si in the support. We obtain ohmic conduction from the support layer to the CNT forest, where CVD conditions (silicidation) increase the conductivity of the stack.

ACKNOWLEDGMENTS

We acknowledge funding from the EU Integrated Project ‘‘Technotubes’’ under Grant No. 228579. We acknowledge the Helmholtz-Zentrum-Berlin BESSY II synchrotron and we thank the BESSY staff for continuous support.

- ¹B. Q. Wei, R. Vajtai, and P. M. Ajayan, *Appl. Phys. Lett.* **79**, 1172 (2001).
- ²F. Kreupl, A. P. Graham, G. S. Duesberg, W. Steinhögl, M. Liebau, E. Unger, and W. Hoenlein, *Microelectron. Eng.* **64**, 399 (2002).
- ³J. Robertson, G. Zhong, S. Hofmann, B. C. Bayer, C. S. Esconjauregui, H. Telg, and C. Thomsen, *Diamond Relat. Mater.* **18**, 957 (2009).
- ⁴M. Nihei, A. Kawabata, and Y. Awano, *Jpn. J. Appl. Phys.* **42**, L721 (2003).
- ⁵M. Nihei, M. Horibe, A. Kawabata, and Y. Awano, *Jpn. J. Appl. Phys.* **43**, 1856 (2004).
- ⁶M. Nihei, A. Kawabata, D. Kondo, M. Horibe, S. Sato, and Y. Awano, *Jpn. J. Appl. Phys.* **44**, 1626 (2005).
- ⁷M. Katagiri, N. Sakuma, Y. Yamazaki, M. Suzuki, S. Sato, M. Nihei, T. Sakai, and Y. Awano, *Jpn. J. Appl. Phys.* **48**, 090205 (2009).
- ⁸Y. Yamazaki, M. Katagiri, N. Sakuma, M. Suzuki, T. Sakai, S. Sato, M. Nihei, and Y. Awano, *Appl. Phys. Exp.* **3**, 055002 (2010).
- ⁹J. Dijon, A. Fournier, P. D. Szkutnik, H. Okuno, C. Jayet, and M. Fayolle, *Diamond Relat. Mater.* **19**, 382 (2010).
- ¹⁰J. Dijon, H. Okuno, M. Fayolle, T. Vo, J. Pontcharra, D. Acquaviva, D. Bouvet, A. M. Ionescu, C. S. Esconjauregui, B. Capraro, E. Quesnel, and J. Robertson, *Tech. Dig. – Int. Electron Devices Meet.* 33.4.1 (2010).
- ¹¹G. D. Nessim, M. Seita, K. P. O’Brien, A. J. Hart, R. K. Bonaparte, R. R. Mitchell, and C. V. Thompson, *Nano Lett.* **9**, 3398 (2009).
- ¹²K. Hata, D. N. Futaba, K. Mizuno, T. Namai, M. Yumura, and S. Iijima, *Science* **306**, 1362 (2004).
- ¹³Y. Murakami, S. Chiashi, Y. Miyauchi, M. Hu, M. Ogura, T. Okubo, and S. Maruyama, *Chem. Phys. Lett.* **385**, 298 (2004).
- ¹⁴G. Zhong, T. Iwasaki, K. Honda, Y. Furukawa, I. Ohdomari, and H. Kawarada, *Jpn. J. Appl. Phys.* **44**, 1558 (2005).
- ¹⁵G. Zhong, T. Iwasaki, J. Robertson, and H. Kawarada, *J. Phys. Chem. B* **111**, 1907 (2007).
- ¹⁶Y.-Q. Xu, E. Flor, M. J. Kim, B. Hamadani, H. Schmidt, R. E. Smalley, and R. H. Hauge, *J. Am. Chem. Soc.* **128**, 6560 (2006).
- ¹⁷S. Noda, K. Hasegawa, H. Sugime, K. Takehi, Z. Zhang, S. Maruyama, and Y. Yamaguchi, *Jpn. J. Appl. Phys.* **46**, L399 (2007).
- ¹⁸M. Cantoro, S. Hofmann, S. Pisana, V. Scardaci, A. Parvez, C. Ducati, A. C. Ferrari, A. M. Blackburn, K.-Y. Wang, and J. Robertson, *Nano Lett.* **6**, 1107 (2006).
- ¹⁹C. Zhang, S. Pisana, C. T. Wirth, A. Parvez, C. Ducati, S. Hofmann, and J. Robertson, *Diamond Relat. Mater.* **17**, 1447 (2008).
- ²⁰C. T. Wirth, C. Zhang, G. Zhong, S. Hofmann, and J. Robertson, *ACS Nano* **3**, 3560 (2009).
- ²¹T. Yamada, T. Namai, K. Hata, D. N. Futaba, K. Mizuno, J. Fan, M. Yudasaka, M. Yumura, and S. Iijima, *Nat. Nanotechnol.* **1**, 131 (2006).
- ²²T. de los Arcos, F. Vonau, M. G. Garnier, V. Thommen, H.-G. Boyen, P. Oelhafen, M. Dueggelin, D. Mathis, and R. Guggenheim, *Appl. Phys. Lett.* **80**, 2383 (2002).
- ²³Y. Wang, B. Li, P. S. Ho, Z. Yao, and L. Shi, *Appl. Phys. Lett.* **89**, 183113 (2006).
- ²⁴Y. Wang, Z. Luo, B. Li, P. S. Ho, Z. Yao, L. Shi, E. N. Bryan, and R. J. Nemanich, *J. Appl. Phys.* **101**, 124310 (2007).

- ²⁵S. Esconjauregui, B. C. Bayer, M. Fouquet, C. T. Wirth, C. Ducati, S. Hofmann, and J. Robertson, *Appl. Phys. Lett.* **95**, 173115 (2009).
- ²⁶C. Zhang, F. Yan, C. S. Allen, B. C. Bayer, S. Hofmann, B. J. Hickey, D. Cott, G. Zhong, and J. Robertson, *J. Appl. Phys.* **108**, 024311 (2010).
- ²⁷B. C. Bayer, S. Hofmann, C. Castellarin-Cudia, R. Blume, C. Baetz, S. Esconjauregui, C. T. Wirth, R. A. Oliver, C. Ducati, A. Knop-Gericke, R. Schlögl, A. Goldoni, C. Cepek, and J. Robertson, *J. Phys. Chem. C* **115**, 4359 (2011).
- ²⁸C. Jin, M. Delmas, P. Aubert, F. Alvarez, T. Minéa, M. C. Hugon, and B. Bouchet-Fabre, *Thin Solid Films* **519**, 4095 (2011).
- ²⁹S. Esconjauregui, B. C. Bayer, M. Fouquet, C. T. Wirth, F. Yan, R. Xie, C. Ducati, C. Baetz, C. Castellarin-Cudia, S. Bhardwaj, C. Cepek, S. Hofmann, and J. Robertson, *J. Appl. Phys.* (in press, 2011).
- ³⁰K. Maex, *Mater. Sci. Eng. R* **11**, 53 (1993).
- ³¹E. G. Colgan, J. P. Gambino, and Q. Z. Hong, *Mater. Sci. Eng. R* **16**, 43 (1996).
- ³²J. P. Gambino and E. G. Colgan, *Mater. Chem. Phys.* **52**, 99 (1998).
- ³³*Metal Based Thin Films for Electronics*, edited by K. Wetzig and C. M. Schneider, 2nd ed. (Wiley-VCH Verlag, Weinheim, Germany 2006).
- ³⁴S.-L. Zhang and M. Oestling, *Crit. Rev. Solid State Mater. Sci.* **28**, 1 (2003).
- ³⁵C. Lavoie, F. M. d'Heurle, C. Detavernier, and C. Cabral, *Microelectron. Eng.* **70**, 144 (2003).
- ³⁶C. Lavoie, C. Detavernier, C. Cabral, F. M. d'Heurle, A. J. Kellock, J. Jordan-Sweet, and J. M. E. Harper, *Microelectron. Eng.* **83**, 2042 (2006).
- ³⁷S. V. Meschel and O. J. Kleppa, *J. Alloys Compd.* **321**, 183 (2001).
- ³⁸C. Mattevi, C. T. Wirth, S. Hofmann, R. Blume, M. Cantoro, C. Ducati, C. Cepek, A. Knop-Gericke, S. Milne, C. Castellarin-Cudia, S. Dolafi, A. Goldoni, R. Schloegl, and J. Robertson, *J. Phys. Chem. C* **112**, 12207 (2008).
- ³⁹S. Hofmann, R. Blume, C. T. Wirth, M. Cantoro, R. Sharma, C. Ducati, M. Haevecker, S. Zafeiratos, P. Schnoerch, A. Oesterreich, D. Teschner, M. Albrecht, A. Knop-Gericke, R. Schloegl, and J. Robertson, *J. Phys. Chem. C* **113**, 1648 (2009).
- ⁴⁰A. Knop-Gericke, E. Kleimenov, M. Hävecker, R. Blume, D. Teschner, S. Zafeiratos, R. Schlögl, V.I. Bukhtiyarov, V.V. Kaichev, I.P. Prosvinin, A. I. Nizovski, H. Bluhm, A. Barinov, P. Dudin, and M. Kiskinova, *Adv. Catal.* **52**, 213 (2009).
- ⁴¹Note that in all CVD conditions the growth time (>20 min) exceeds the constant growth rate regime and the forest height of tens of μm is due to self-termination of growth.
- ⁴²Powder Diffraction Files, JCPDS-International Centre for Diffraction Data, Newtown Square, PA; poly-Si: 27-1402, CoSi₂: 38-1449, CoSi: 50-1337, CoO: 89-2803, Co₂SiO₄: 29-0506.
- ⁴³S.C. Petitto, E. M. Marsh, G. A. Carson, and M. A. Langell, *J. Mol. Catal. A: Chem.* **281**, 49 (2008).
- ⁴⁴G. Hollinger, *Appl. Surf. Sci.* **8**, 318 (1981).
- ⁴⁵T. P. Nguyen and S. Lefrant, *J. Phys.: Condens. Matter* **1**, 5197 (1989).
- ⁴⁶M. Aronniemi, J. Sainio, and J. Lahtinen, *Surf. Sci.* **578**, 108 (2005).
- ⁴⁷M. Descostes, F. Mercier, N. Thromat, C. Beaucaire, and M. Gautier-Soyer, *Appl. Surf. Sci.* **165**, 288 (2000).
- ⁴⁸R. Reiche, F. Yubero, J.P. Espinos, and A.R. Gonzalez-Elipe, *Surf. Sci.* **457**, 199 (2000).
- ⁴⁹W. Platow, D. K. Wood, K. M. Tracy, J. E. Burnette, R. J. Nemanich, and D. E. Sayers, *Phys. Rev. B* **63**, 115312 (2001).
- ⁵⁰We note that with SEM and point localized energy dispersive x-ray spectroscopy (EDX) we found that few large, μm -sized Fe particles are present on parts of the sample surface. These particles are very likely not completely reduced during processing because of their size. While these contaminations are from sample preparation and inactive for growth, they might have artificially increased the non-reduced iron signal. Nevertheless, the much larger sampled area of Co-silicide compared to the surface of the few Fe-particles indicates that the high Fe-oxide signal during processing is from a genuine interface effect. Furthermore, already without C₂H₂ exposure a small FeC component is visible in the Fe2p when heating the samples. We attribute this to interactions with adventitious carbon from transport in ambient air (Ref. 51).
- ⁵¹I. N. Shabanova and V. A. Trapeznikov, *J. Electron Spectrosc. Relat. Phenom.* **6**, 297 (1975).
- ⁵²S. Esconjauregui, C. M. Whelan, and K. Maex, *Nanotechnology* **18**, 015602 (2007).
- ⁵³E. Flahaut, A. Govindaraj, A. Peigney, C. Laurent, A. Rousset, and C. N. R. Rao, *Chem. Phys. Lett.* **300**, 236 (1999).
- ⁵⁴W.-H. Chiang and R. M. Sankaran, *Nature Mater.* **8**, 882 (2009).
- ⁵⁵W.-H. Chiang and R. M. Sankaran, *Adv. Mater.* **20**, 4857 (2008).
- ⁵⁶S. Esconjauregui, M. Fouquet, B. C. Bayer, S. Eslava, S. Khachadorian, S. Hofmann, and J. Robertson, *J. Appl. Phys.* **109**, 044303 (2011).
- ⁵⁷S. Esconjauregui, M. Fouquet, B. C. Bayer, C. Ducati, R. Smajda, S. Hofmann, and J. Robertson, *ACS Nano* **4**, 7431 (2010).